Multiepoch Grid-Based 3DMA Positioning in Dense Urban Canyons by Optimizing Reflection Modeling

Huan Luo, Xiaolong Mi, Yang Yang, Wu Chen, and Duojie Weng

***Abstract*— Urban positioning with global navigation satellite systems (GNSSs) poses a significant challenge due to signal reflections, diffractions, and obstructions caused by surroundings. These factors introduce multipath interference and non-line of sight (NLOS) signal reception, leading to a degradation in positioning accuracies up to tens of meters. The growing accessibility of 3-D city models offers an opportunity for modeling and analyzing the effects of multipath and NLOS on GNSS signals. 3-D mapping aided (3DMA) methods have shown effectiveness in positioning improvement by correcting NLOS delays in preliminary research. However, without consideration of diffractions, which frequently occurs in urban canyons, the usable satellites from simulation are significantly reduced in their methods. Moreover, the conventional positioning scheme lacks robustness when receivers suffer from unmodeled errors and dynamic interference. In this contribution, we propose an enhanced 3DMA ray-tracing (RT) algorithm (RT-based grid weight smoothing and clustering, RT-GWSC). This method incorporates a reflection–diffraction (RD) model, and it introduces a positioning scheme with multiepoch weight smoothing and density-based spatial clustering of applications with noise (DBSCAN) clustering approach. The performance has been evaluated with different urban environments in both static and kinematic experiments. The results demonstrated that the RD model outperforms the conventional reflection model, with a significant improvement in sensitivity of NLOS prediction from 53.7% to 90.7% and overall accuracy from 86.3% to 96.8%. Overall, the RT-GWSC method could reduce outliers in positioning stage and achieve positioning accuracies better than 15 m in all tested environments, outperforming raw GNSS outputs with improvement rates (IRs) over 73%, while the conventional RT approach was found ineffective in certain complicated environments.**

***Index Terms*— 3-D city model, global navigation satellite system (GNSS) positioning, low-cost devices, multipath effects, non-line of sight (NLOS) correction.**

Received 25 July 2024; revised 9 October 2024; accepted 4 November 2024. Date of publication 25 February 2025; date of current version 11 March 2025. This work was supported in part by the Research Grants Council of Hong Kong through the General Research Fund under Grant 15229622 and Grant 15230823. The Associate Editor coordinating the review process was Dr. Yulong Huang. *(Corresponding author: Duojie Weng.)*

Huan Luo, Xiaolong Mi, and Yang Yang are with the Department of Land Surveying and Geo-Informatics, The Hong Kong Polytechnic University, Hong Kong (e-mail: hilary.luo@connect.polyu.hk; xiaolong.mi@polyu.edu.hk; yyoung.yang@polyu.edu.hk).

Wu Chen is with the Research Institute for Artificial Intelligence of Things and the Department of Land Surveying and Geo-Informatics, The Hong Kong Polytechnic University, Hong Kong (e-mail: wu.chen@polyu.edu.hk).

Duojie Weng is with the Ministry of Natural Resources (MNR) Key Laboratory for Geo-Environmental Monitoring of Great Bay Area and Guangdong Key Laboratory of Urban Informatics, Shenzhen University, Shenzhen 518060, China, and also with the Department of Land Surveying and Geo-Informatics, The Hong Kong Polytechnic University, Hong Kong (e-mail: djweng@szu.edu.cn).

Digital Object Identifier 10.1109/TIM.2025.3545163

I. Introduction

URBAN positioning has emerged as a critical component in modern society, particularly with the growing reliance on location-based services, intelligent transportation systems, autonomous driving, and navigation systems [1], [2], [3]. Global navigation satellite system (GNSS) is the most widely used technology for obtaining location information, providing location services for the mass market with consumer-level receivers [4], [5], [6]. However, the performance of GNSS is significantly compromised in urban environments, where the high-rise buildings and dense infrastructure cause the reflection, diffraction, and blockage of GNSS signals [7]. Receiving both direct and reflected signals introduces multipath interference, while receiving only reflected signals leads to non-line-of-sight (NLOS) reception [8]. Consequently, the corresponding positioning errors can be deteriorated up to tens of meters [9]. Additionally, the urban environments can result in poor satellite geometry, further degrading the positioning accuracy.

Several techniques have been proposed to mitigate multipath interference and/or NLOS reception. One approach to address these issues is through antenna and/or receiver design [10], [11], [12], [13], [14], [15], [16], [17]. Advanced antenna can minimize the reception of reflected GNSS signals, and innovative receiver designs can incorporate signal processing algorithms and filtering methods, reducing the impact of multipath interference. However, these techniques require customization of hardware, which can increase the cost and size of devices, and demand more power, making them unsuitable for ready-to-use devices. Without additional hardware or materials, consistency checking is a widely used approach for detecting and mitigating errors of multipath and NLOS signals [18], [19], [20], [21], [22], [23]. Consistency checking enhances the reliability of GNSS positioning solutions by detecting and isolating contaminated signals via redundant satellite measurements. With the street constraints, the performance of consistency check can be improved in dense urban areas [24]. However, it faces several challenges in mitigating multipath effects in urban canyons. The line-of-sight (LOS) signal is easily obstructed by dense buildings and/or multiple satellites can provide distorted signals. These complex environments impair the ability of consistency checking to detect and isolate faulty free measurements. Even when consistency checking successfully identifies and excludes faulty signals, the geometry of remaining signals may still be poor, decreasing the positioning performance [25]. Consistency checking presents a significant challenge in urban positioning, and

1557-9662 © 2025 IEEE. All rights reserved, including rights for text and data mining, and training of artificial intelligence and similar technologies. Personal use is permitted, but republication/redistribution requires IEEE permission.
See https://www.ieee.org/publications/rights/index.html for more information.
Authorized licensed use limited to: Hong Kong Polytechnic University. Downloaded on June 16,2025 at 12:40:55 UTC from IEEE Xplore. Restrictions apply.

therefore, several methods and technologies are being explored and developed.

High-rise buildings and infrastructures are the primary contributors to multipath effects. Therefore, a 3-D city model can aid in predicting the paths of GNSS signal, and the wide availability of 3-D models provides a solution to mitigate the impact of multipath errors. By constructing 3-D models of buildings and infrastructures, it is possible to predict the paths of GNSS signals, allowing the estimation and correction of multipath errors. One 3DMA-based approach is shadow matching, which matches the measured signal patterns with the patterns of signal visibility prediction based on a 3-D model and receiver's position [26], [27], [28], [29], [30], [31], [32]. This technique can assist in locating the user on the correct side of the street, thereby enhancing cross-street positioning accuracy in urban canyons. However, its effectiveness diminishes with increasing street width and decreases along the street direction. Besides, although it accounts for signal blockage, it may still be challenged by signal reflections and diffractions. Another technique is based on ray tracing (RT), which provides a more comprehensive analysis of signal propagation [33], [34], [35], [36], [37]. It simulates the travel paths of GNSS signals through surroundings defined by a 3-D model, and compares the received pseudoranges and predicted signal path values. In urban canyons, since the initial GNSS positioning error is large, a particle matching approach was proposed to improve the efficiency of RT-based methods, which generates particles based on GNSS conventional solutions and assumes that the best agreement of received and simulated path delays should be at the true point [38], [39], [40], [41]. Additionally, RT technology was extended to GNSS velocity estimation on Doppler observations, which exhibited its feasibility on Doppler frequency correction [42]. Considering the high computational loads and/or the absence of 3-D models, some studies have employed additional hardware. Lyu and Gao [43] proposed a pixel shader-based RT method for NLOS correction with an omnidirectional camera to reduce the computational demands. Some studies employed light detection and ranging (LiDAR) or a fisheye camera to reconstruct the surroundings for NLOS detection and correction [44], [45]. Moreover, 3DMA technologies have been extended to the seamless positioning with the integration of inertial sensors [46].

Several studies have shown that the RT approaches are effective to improve the horizontal positioning accuracy. These studies primarily focused on analyzing reflection signals while neglecting the occurrence of the diffraction phenomenon. In reality, diffraction often occurs in urban canyons, significantly affecting signal behavior and propagation [47]. Therefore, it is essential to consider both reflection and diffraction phenomena during the prediction phase to ensure a comprehensive understanding of signal propagation in urban environments. Furthermore, besides the effects from buildings and infrastructures, satellite signals can be easily affected by moving objects in urban regions. Vehicles and pedestrians moving through the environments can create temporary signal blockages, reflection or diffraction, especially when these objects are almost relatively static to the receiver. These interruptions can cause fluctuations in strength and quality of received signals, or directly introduce reflected or diffracted signals. The unmodeled errors remained in observations would affect the accuracy of grid weight calculations. The conventional RT approach fails to account for these interferences caused by pedestrians and vehicles. Its performance is also affected by the accuracy of the 3-D model. Additionally, there are still some unmodeled errors from low-cost devices. These factors contribute to the unreliability and lack of robustness of positioning solutions. Consequently, there is a need for a robust positioning scheme to provide more reliable solutions. This article builds upon the conventional RT approach to further enhance both the accuracy and robustness of positioning. The main contributions are listed below.

1) A novel reflection model incorporating a more comprehensive analysis of signal propagation is introduced. Addressing the limitation of the lack of the diffraction signal estimation, the success rate of estimation can be improved.
2) A novel positioning scheme, named as the RT-based grid weight smoothing and clustering (RT-GWSC) method, is proposed. By integrating multiepoch GNSS measurements and inertial sensor data, the grid weights can be smoothed. It can effectively mitigate the effects of unmodeled errors. By utilizing the density-based spatial clustering of applications with noise (DBSCAN) clustering approach in position domain with filtered weights, the positioning performance can be further enhanced, especially for its reliability and robustness.
3) Extensive tests have been conducted in urban canyons in both static and kinematic cases. Results firstly show that the enhanced signal simulation approach outperforms the traditional method with a higher success rate of classification. Secondly, the proposed technique achieves a valuable enhancement in GNSS positioning accuracy and reliability, both in static and kinematic tests conducting in typical dense urban areas.

The rest of this article is structured as follows: a brief introduction and methodology of the proposed method are outlined in Section II. Section III presents the experimental setup and results for validating and assessing the proposed method. The conclusion and future works are summarized in Section IV.

II. Methodology

A. Algorithm Framework

The overall structure of the proposed RT-based approach has been illustrated in Fig. 1. Firstly, the received pseudorange residuals of all satellites are calculated with utilizing GNSS measurements, satellite ephemeris, and ground point coordinates. Then, the signal path delay is predicted with 3-D city model and ground point, and the corresponding pseudorange residuals among simulation are determined. Afterward, the residuals between reception and simulation are differenced for weight calculation of ground points. Finally, positioning results are solved by the grid weighting and DBSCAN clustering approaches.

Building on the conventional RT-based method, this article proposes two improved algorithms, colored in blue in Fig. 1, including a reflection–diffraction (RD) model and a novel positioning scheme. The simulation of path delays among

Authorized licensed use limited to: Hong Kong Polytechnic University. Downloaded on June 16,2025 at 12:40:55 UTC from IEEE Xplore. Restrictions apply.

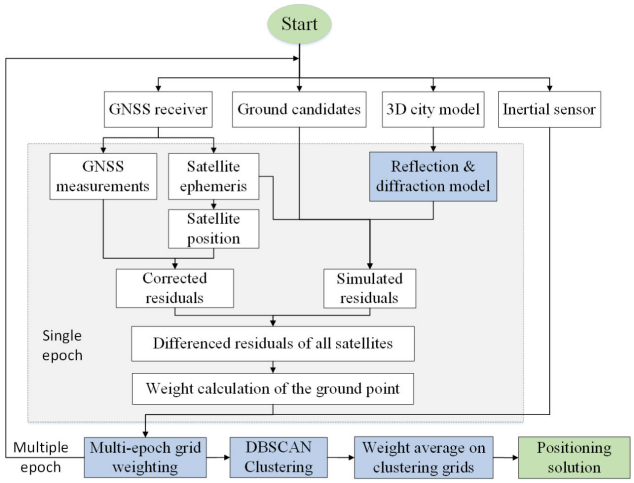

Fig. 1. Structure of the improved RT-based approach.

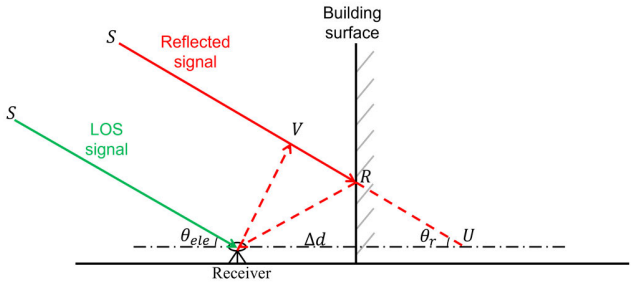

Fig. 2. Illustration of a satellite signal reflection.

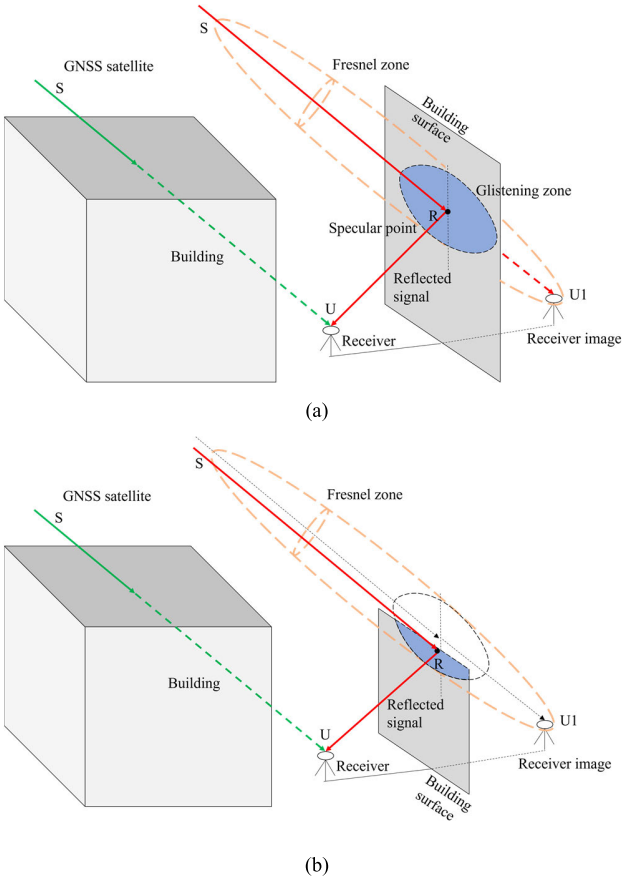

Fig. 3. Illustration of the satellite signal reflection in two scenarios. (a) Specular point is situated on the building surface. (b) Specular point falls outside the building surface.

all received satellite signals is one key part in the 3DMA-based approach. Based on the geometry of satellites, the receiver and building planes, the travel path of signals can be generated. For NLOS signals, the path delays are predicted by the reflection model. In the conventional RT-based approach, only reflection phenomenon is considered. Different from the conventional approach, the RD model considers both the reflection and diffraction phenomenon to improve the simulation rate of NLOS signals. After the calculation of grid weights, the proposed technique introduces the multiepoch grid-based approach in the positioning phase. Multiepoch data of GNSS and inertial sensor data are involved to smooth the grid weight, rather than the use of single epoch data in the conventional method. In case of outliers with high weights, which deviate from the true location, the performance of conventional method is easily affected. In contrast, the DBSCAN clustering method, which can recognize clusters and outliers/noise within a spatial database set, is utilized to categorize effective candidates into groups according to their positions and determine the optimal clusters. Compared to the single epoch-based RT positioning method, the proposed method can enhance the positioning performance and robustness using low-cost devices in urban canyons.

B. Approach of Path Delay Estimation

1) Signal Reflection Hypothesis: In the conventional RT-based approach, RT is a commonly employed technique for estimating signal path delays. In this method, reflected signals are assumed to adhere to geometrical optics principles, with the behavior of RT following the law of specular reflection [38], [48], as shown in Fig. 2.

From Fig. 2, the path of GNSS signal in simulation is represented as follows:

$$\rho_s = \mathrm{SR} + \mathrm{RU} = \mathrm{SU} + D \tag{1}$$

where ρ_s denotes the predicted path of reflected satellite signal, RU and SR represent the paths from the specular reflection point to the receiver and satellite, respectively; D is the NLOS delay compared to the LOS path (SU).

For most cases, the building surfaces are vertical to the ground, and the signal is assumed to be reflected as Fig. 2. In this case, the path delay of reflected point D can be calculated by the distance Δd between the receiver and the building surface and the incidence angle θ_r, with the equation of $2 \cdot \Delta d \cdot \cos(\theta_r)$. However, it should be noted that the incidence angle is not strictly θ_r when the surface is non-vertical such as building surfaces from skyscrapers. The incidence angle is the sum of θ_r and inclination angle of the building surface $\delta\theta$. Considering the inclination angle is generally small, we can assume $\cos(\theta_r + \delta\theta) \approx \cos(\theta_r)$. Hence, $\delta\theta$ is neglectable in current approach.

Theoretically, the overall reflected signal is derived from an area of reflecting surface, rather than originating from a single point as defined in conventional RT methods. In Fig. 3(a), the ellipsoid (highlighted in orange) symbolizes the Fresnel zone. This zone is characterized as an ellipsoidal area where objects contained within it can impact signal propagation, potentially

Authorized licensed use limited to: Hong Kong Polytechnic University. Downloaded on June 16,2025 at 12:40:55 UTC from IEEE Xplore. Restrictions apply.

causing constructive and destructive interference. The region (depicted in blue), which is formed by the intersection of the first Fresnel zone with the reflecting surface, is the main source of the reflected signal power. In scenarios where the receiver antenna is near the reflecting surface, such as ground-based stations, the direct GNSS signal can be considered as nearly parallel to both the receiver antenna and the reflecting surface, as shown in Fig. 3(a). When the reflecting surface is assumed to be a plane, the semi-major axis and the semi-minor axis of the first Fresnel zone can be calculated [49].

In situations where the specular reflection point is situated outside the building surface, effective reflection can still occur if the zone partially overlays with the building surface. This could elucidate why RT is prone to failure when attempting to simulate the propagation path in these scenarios, as shown in Fig. 3(b).

Two distinct scenarios emerge when calculating the position of the specular reflection point due to the geometric considerations.

1) When the specular reflection point is within the building surface [as depicted in Fig. 3(a)], which is defined as the point of intersection where the line connecting the satellite to the image of the receiver intersects with the building surface, this particular point is recognized as the reflection point for the satellite.
2) When the specular reflection point is outside the building surface, as shown in Fig. 3(b), the Fresnel zone is identified (highlighted in blue region). The reflection point is determined by selecting the point in the region nearest to the specular reflection point.

The visibility of reflection point is confirmed through their geometry. A functional reflection point is confirmed with visibility to both the receiver and the satellite. By establishing the valid reflection point (R), it enables the prediction of multipath and NLOS delay referring to (1).

Based on this hypothesis, the types of signal reception can be classified into three categories: LOS, NLOS-with-reflection (the LOS is blocked by a building but the signal can arrive at the receiver through reflection from a building surface), and NLOS-without-reflection (the LOS is obstructed but no valid reflection is found), as the previous research [50].

2) Algorithm Description: As discussed in Section II-B1, an RD model for simulating reflected signals is proposed here, and the algorithm is described in Algorithm 1, with the assistance of a 3-D city map.

Algorithm 1 Procedures of Path Delay Calculation

Input

Grid point list, GNSS measurements, 3D city model

Procedures

Initial position → search region
  for *Each grid point* **in** *Grid point list* **do**
    for *Each satellite* **in** *Received satellite list* **do**
      for *Each plane* **in** all building planes ← *building region* **do**
        if *grid point* $\overset{visible}{\longleftrightarrow}$ *satellite*
          LOS, ***no path delay***
        else
          Calculate *grid point, satellite, building plane* → mirror point → specular point
        if *specular point* **on** *building plane*
          specular point → reflection point
        else
          if *specular point* in *Fresnel region*
            The nearest point in Fresnel → reflection point
          else
            No reflection point
          end
        end
        if *grid point* $\overset{visible}{\longleftrightarrow}$ *reflection point, satellite* $\overset{visible}{\longleftrightarrow}$ *reflection point*
          NLOS-with-reflection
          Calculate *grid point, satellite, reflection point* → ***path delay***
        else
          NLOS-without-reflection; ***No path delay***
        end
      end
    end
  end
end

Output

Path delay of all satellites on each grid

C. Positioning Scheme

1) Weight Calculation of Grid Points: GNSS observations are subject to several types of errors, such as satellite clock errors, receiver clock errors, tropospheric delays, ionospheric delays, multipath effects, and noises. The fundamental equation for code measurements can be represented mathematically as follows:

$$P_r^s(t) = \rho + T + I + c\left(\delta t_r - \delta t^S\right) + M + n \tag{2}$$

where ρ represents the distance between satellite and receiver, T denotes the tropospheric delay, I indicates the ionospheric delay, δt_r and δt^S represent the clock error of receiver and satellite, respectively, M denotes the multipath delay, and n is the noise.

In this article, the troposphere and ionosphere error are eliminated using Hopfield two quartic model [51] and Klobuchar model [52], respectively, while the satellite clock error is removed using polynomial estimation. After the elimination of above errors, the corrected measurement is expressed as follows:

$$P_r^s(t)_{\text{corrected}} = \rho + c\delta t_r + M + n. \tag{3}$$

The satellite with the highest elevation angle and SNR is then chosen as the reference satellite to eliminate the receiver clock error, where it is assumed that the reference satellite is not affected by multipath effect. The single difference (SD) between satellites can be expressed as follows:

$$\begin{aligned} P_r^s(t)^{\text{SD}}_{\text{corrected}} &= P_r^s(t)_{\text{corrected}} - P_r^{s_{\text{ref}}}(t)_{\text{corrected}} \\ &= \left(\rho^S + M^S + n^S\right) - \left(\rho^{s_{\text{ref}}} + M^{s_{\text{ref}}} + n^{s_{\text{ref}}}\right) \end{aligned} \tag{4}$$

where $M^{s_{\text{ref}}}$ is assumed to be zero.

Authorized licensed use limited to: Hong Kong Polytechnic University. Downloaded on June 16,2025 at 12:40:55 UTC from IEEE Xplore. Restrictions apply.

In the research of the quality assessment of GNSS receivers, the measurement noises of pseudorange received from geodetic receivers and low-cost receivers (u-blox) are below 0.35 m [53]. In urban environments, errors caused by multipath effects range from tens to hundreds of meters [54]. The difference between measurement noises from GNSS receivers and multipath errors is 2–3 orders of magnitude. Therefore, the measurement noise can be neglected in pseudorange. Referring to (4), the SD observations can then be written as follows:

$$P_r^s(t)^{\mathrm{SD}}_{\mathrm{corrected}} = \left(\rho^S + M^S\right) - \rho^{s_{\mathrm{ref}}}. \tag{5}$$

The signal path for a known ground point can be estimated with the RD model, and the corresponding satellite signal path can be simulated through the following:

$$P^S_{\mathrm{simulated}} = \rho^S + M^S_{\mathrm{simulated}}. \tag{6}$$

Similar to measurements, the SD of simulated travel distance, following the same procedure as described in (5), can be stated as follows:

$$P_r^s(t)^{\mathrm{SD}}_{\mathrm{simulated}} = \left(\rho^S + M^S_{\mathrm{simulated}}\right) - \left(\rho^{s_{\mathrm{ref}}} + M^{s_{\mathrm{ref}}}_{\mathrm{simulated}}\right). \tag{7}$$

Combining (5) and (7), the two SDs give the double difference (DD) between pseudorange and simulated travel distance. This DD value is used as an index for the similarity between the true point and the chosen point, expressed as follows:

$$\Delta\nabla P = P_r^s(t)^{\mathrm{SD}}_{\mathrm{corrected}} - P_r^s(t)^{\mathrm{SD}}_{\mathrm{simulated}} \tag{8}$$

where $\Delta\nabla P$ denotes the DD between SD of reception and SD of simulation.

The pseudorange similarities for all candidates can be normalized, represented as follows:

$$\Delta\nabla\hat{P} = \mathrm{Normalize}(\Delta\nabla P) \tag{9}$$

where Normalize() indicates the normalize function.

The weight for each candidate is calculated as follows:

$$W_{C_j} = \frac{\sum_N \Delta\nabla\hat{P}_{S_N}}{N} \tag{10}$$

where C_j represents the jth point, and N denotes the pseudoranges index.

2) Multiepoch Grid Weight Filter: To mitigate the effects from the remained errors in pseudorange residuals, the proposed approach incorporates a multiepoch weight filter, consisting of two steps: grid mapping and weight filtering. With the use of inertial sensors, the relative position of the receiver can be calculated. The relative movements between two consecutive epochs can be computed, which has been studied in our previous research [55], as follows:

$$\begin{cases} \Delta N_i = \mathrm{SL}_{i-1} \cdot \mathrm{SN}_i \cdot \cos\theta_i \\ \Delta E_i = \mathrm{SL}_{i-1} \cdot \mathrm{SN}_i \cdot \sin\theta_i \end{cases} \tag{11}$$

where ΔN and ΔE represent the changes in northing and easting coordinates of the pedestrian, the subscript i corresponds to time, SL stands for step length, SN denotes step number, and θ signifies the heading direction of the pedestrian.

Between two epochs, the cumulative movement changes can be described as follows:

$$\begin{cases} \Delta N_{ij} = \sum_{j}^{t=i} \Delta N_t \\ \Delta E_{ij} = \sum_{j}^{t=i} \Delta E_t \end{cases} \tag{12}$$

where subscript t, i, and j denotes the time.

Subsequently, the grid at epoch i is mapped to epoch j as an a priori condition, and the mapping function can be expressed as follows:

$$\begin{cases} \Delta\mathrm{GN}_{ij} = \mathrm{mod}(\Delta N_{ij}, \mathrm{Int}V) \\ \Delta\mathrm{GE}_{ij} = \mathrm{mod}(\Delta E_{ij}, \mathrm{Int}V) \end{cases} \tag{13}$$

where ΔGN and ΔGE denote the grid movements between two epochs, and Int$V$ is the grid interval.

Additionally, the grid weights of previous epochs can be correspondingly mapped to the current epoch, expressed as follows:

$$W_{C_t} \rightarrow W_{C_{tj}}. \tag{14}$$

In a consecutive period $a, b, \ldots, j$, a list of weight for a grid can be matched, expressed as $W_{C_{aj}}, W_{C_{bj}}, \ldots, W_{C_{jj}}$. Subsequently, the grid weight in time j can be refined within the measurement domain. Taking into account the accumulated error with time in pedestrian dead reckoning (PDR) technique, the PDR result of later epoch has higher accuracy than the earlier one with longer accumulation. By applying exponentially weighted moving average (EWMA), which can be easily employed with small computation, a list of weights can be organized better. In EWMA, the weighting of each older data decreases exponentially, while the weight of the newest data remains higher, that is, the effect from previous accumulated data significantly reduced. The EWMA approach is utilized as demonstrated by the following:

$$\begin{cases} \overline{W_{C_j}} = (1-\beta)W_{C_{jj}} + \beta\overline{W_{C_{j-1}}} \\ \overline{W_{C_0}} = W_{C_{aa}} \end{cases} \tag{15}$$

where β is the smoothing parameter.

β is an empirical parameter, which is calculated by half of the grid interval as the error limitation, error ratio of PDR system, and the step length of the pedestrian.

The weight of each grid is ultimately refined in time series, substituting W_{C_j} in grid-based weighting methodologies.

3) DBSCAN Clustering Positioning: In various research works, the positioning solutions are typically established using the likelihood-based method on all candidates or eligible candidates meeting specific criteria [27], [38]. Under ideal circumstances, the weighted average (WA) on the positions of eligible candidates closely aligns with the ground truth. However, if some errors persist in measurement residuals from certain satellites, the associated candidate weights may be inaccurate, which potentially leads to outliers significantly deviating from the ground truth. Although the weight smoothing approach can largely mitigate errors, the remained errors, caused by 3-D model errors and multipath effects, can also degrade the WA-based positioning accuracy.

Authorized licensed use limited to: Hong Kong Polytechnic University. Downloaded on June 16,2025 at 12:40:55 UTC from IEEE Xplore. Restrictions apply.

Considering the low likelihood of significant discrepancies between unmodeled errors and position deviations, the amount of outliers is expected to be minimal and isolated. By categorizing candidates with high weights into groups according to their positions, the groups containing the ground truth point are expected to outnumber the others. Consequently, a clustering analysis approach is proposed to categorize these candidates into groups, thereby excluding outliers.

The DBSCAN algorithm, introduced by Ester et al. [56], is a commonly used algorithm for clustering using density. It aims to recognize clusters and outliers/noise within a spatial database set. Two crucial definitions in DBSCAN are the minimum number of neighboring points needed to constitute a cluster (MinPts) and the distance threshold used to determine the connection of neighborhood points (ε(eps)). The clustering result (P_{DBSCAN}) of a point (p) can be expressed as follows:

$$\begin{cases} P_{\text{DBSCAN}}(p) = \{q \in P_{\text{selected}}, D(p,q) < \varepsilon\} \\ \text{Num}(P_{\text{DBSCAN}}(p)) > \text{MinPts} \end{cases} \tag{16}$$

where p and q indicate the points in the selected candidates list (P_{selected}), $D(p,q)$ refers to the distance between two points, ε is the distance threshold, $\text{Num}(P_{\text{DBSCAN}}(p))$ represents the count of points in the clustering group, and MinPts specifies the minimum number of points needed to create a dense region.

Using DBSCAN method, the eligible candidates can be grouped into one or multiple cluster(s), where the candidate count and weight value within each cluster are leveraged to identify the most suitable group. Subsequently, the positioning solution is established based on the chosen group, as illustrated by the following:

$$p(E,N) = \frac{\sum_m W_m \cdot p_m(E,N)}{\sum_m W_m}, \quad (p_m \subset P_{\text{DBSCAN}}) \tag{17}$$

where p_i represents the mth candidate, E and N stand for the easting and northing coordinate, respectively, W denotes the weight computed from (15), P_{DBSCAN} signifies the chosen group determined through the clustering technique.

III. Experiment Results

The experiments were conducted to confirm the feasibility of the proposed approach and validate its accuracies in a complex environment. Field experiments were carried out in one typical site in Hong Kong [Fig. 4(a)], which represents common urban environments with varying degrees of density. The area is characterized by narrow streets and high-rise buildings. A u-blox M8 GNSS model [Fig. 4(b)] was employed as the receiver, with a station from the SatRef network, located close to the rover station, chosen as the base station. The 3-D building model supplied by the survey and mapping office (SMO) of the Hong Kong Lands Department was utilized, with the acknowledgment that it does not include all real-world features such as billboards over the road.

A. Assessment of the RD Model for the Path Delay Estimation

The path delay estimation was assessed through static experiments, where the DD between stations and satellites was conducted to mitigate propagation-related errors, satellite clock errors, and receiver clock errors. Generally, the multipath

(a) (b)

Fig. 4. (a) Experimental environments. (b) GNSS devices: U-blox M8 and antenna.

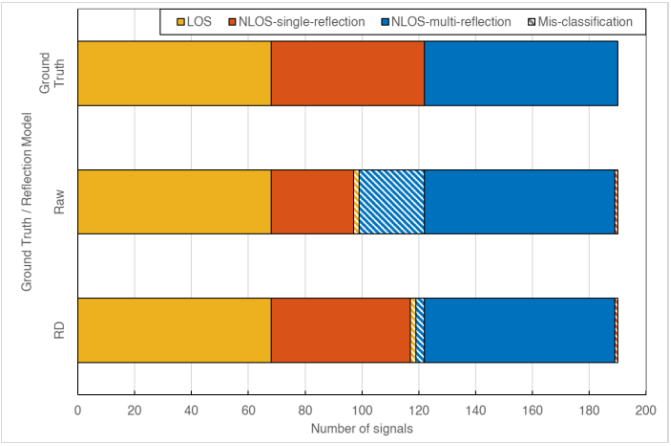

Fig. 5. Comparison of satellite signal classification between the two prediction models.

interference of base station and reference satellite is minor, so the true delays are calculable with the input of the true locations of rover station. The reception classes of satellite signals can be divided into three groups associated with the multipath errors and SNR: LOS, NLOS-with-reflection, and NLOS-without-reflection. The types of simulated signals can subsequently be categorized into three groups with the use of 3-D model. The performance of the RD model for path delay estimation was evaluated by comparing the measured and estimated classification and delays.

From all the data gathered during the experiments, 190 effective signals received at 12 experimental points were analyzed. The classification between reception and simulation is compared in Fig. 5, in which, the predicted classifications from two reflection models (raw and RD) are compared with the reference (ground truth) while the statistics for the results is summarized in Table I. The classes are shown in different colors (yellow: LOS; orange: NLOS-with-reflection; blue: NLOS-without-reflection) with mis-classified signals indicated by shadowing. Both models effectively predicted the true LOS signals, however, two NLOS-with-reflection signals were predicted as LOS, hence, similar performance on LOS signal prediction. Moreover, both models showed similar result in prediction of true NLOS-without-reflection signals with one mis-classified as NLOS-with-reflection. The RD model showed significant improvement in the prediction of NLOS-with-reflection signals (NLOS-with-reflection prediction sensitivity: from 53.7% to 90.7%) with substantial decrease of mis-classification as NLOS-without-reflection from 23 to 3 (NLOS-without-reflection prediction specificity:

Authorized licensed use limited to: Hong Kong Polytechnic University. Downloaded on June 16,2025 at 12:40:55 UTC from IEEE Xplore. Restrictions apply.

TABLE I
ACCURACY OF SATELLITE SIGNAL CLASSIFICATION BETWEEN TWO PREDICTION MODELS

Reflection model	Sensitivity			Specificity			Accuracy
	LOS	NLOS-with-reflection	NLOS-without-reflection	LOS	NLOS-with-reflection	NLOS-without-reflection	
Raw	100.0%	53.7%	98.5%	97.1%	96.7%	74.4%	86.3%
RD	100.0%	90.7%	98.5%	97.1%	98.0%	95.7%	96.8%

*Sensitivity = Correctly predicted class/ true corresponding class;
Specificity = Correctly predicted class/ reported corresponding class;
Accuracy = Correctly predicted classes/ all samples.

from 74.4% to 95.7%). The improved approach has an overall accuracy enhanced from 86.3% to 96.8%.

Utilizing the prediction class of NLOS-with-reflection, the path delays were estimated after identifying the reflected points. These delays were then compared against the observed errors caused by multipath effects. In general, the estimated delays of satellites identified by both the traditional and enhanced models were nearly equivalent. Therefore, the delays obtained from the RD model were utilized for the comparison, as depicted in Fig. 6. The estimated delays show a trend matched with the received errors. The error differences for the other satellites, except for the 22nd which showed a large deviation between reception and prediction, were within 20 m. The detailed analysis of this deviation is discussed in Appendix, explaining the reason why the estimated delay is inconsistent with the received errors. In Fig. 6(b), the cumulative distribution function (cdf) of these error differences is illustrated. More than 95% of signals exhibited estimation errors below 15 m, with more than 65% errors below 5 m.

In conclusion, the RT method proves to be an effective approach for categorizing satellite signals into three reception types. The enhanced RD model demonstrated a higher accuracy in classification. Additionally, the predicted delays are closely equivalent to the actual errors.

B. Evaluation of RT-GWSC Positioning Method

Following the discussion on enhancing the delay estimation approach, the improved positioning technique of RT-GWSC is further assessed as described below. In this section, to evaluate the effectiveness of the proposed method, we conducted three static experiments and one kinematic experiment in Wan Chai, Hong Kong. Observation site 1 was situated on Fleming Road, near the intersection of Fleming and Thomson Road. The width of Fleming Road is 16.5 m, running from north to south. The heights of buildings on two sides are 123.2 and 95 m, with height-to-width (H/W) ratios of 7.5 and 5.8, respectively. Observation site 2 was located on Johnston Road with width of 16.2 m, approximately the same as that of Fleming Road but orientated from east to west. The heights of the buildings on either side of this route are 75 and 33.9 m, with H/W ratios

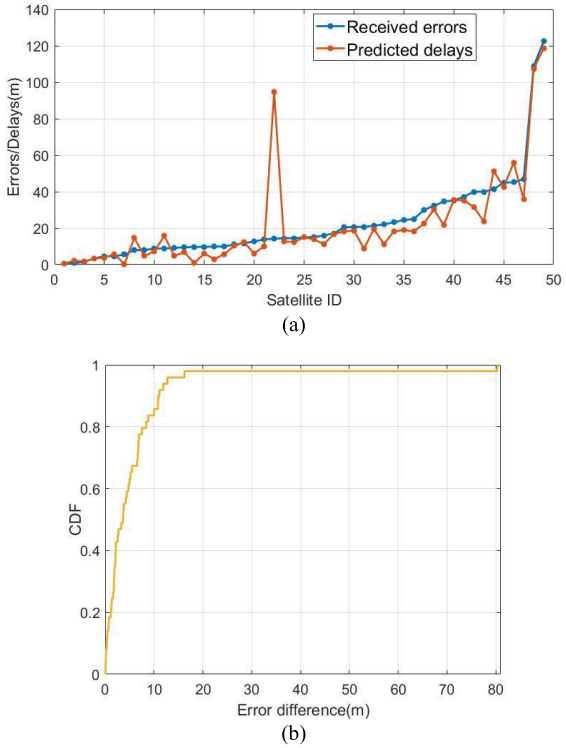

Fig. 6. Comparison of received errors with predicted delays. (a) Comparison of received and predicted values. (b) CDF of the values' error differences.

of 4.6 and 2.1, respectively. Observation site 3 was located on O'Brien Road, of which width is 7.0 m, aligned in the same orientation as Fleming Road. The buildings on either side of this site reach heights of 55 and 68.8 m, resulting in H/W ratios of 7.9 and 9.8, respectively. Additionally, one kinematic experiment was conducted in Wan Chai. The size of the experimental region was approximately 590 $\times$ 100 m^2. The total length of the trajectory is 1247 m, and the observation span was around 22 min. The trajectory is located along Jaff Road, O'Brien Road, and Lockhart Road. The trajectories along the three roads measure 576.7, 56.7, and 613.6 m, with respective widths of 7.4, 15.3, and 15.2 m. The buildings in this area vary in height from 50 to 130 m, with mean building heights along each road recorded at 80, 75, and 80 m, respectively. The corresponding H/W ratios for the buildings are 10.8, 4.9, and 5.3. Data were collected by walking with a u-blox antenna attached to a backpack. Meanwhile, when passing a lamppost, the current time, the detected steps, and the ID of each lamppost, where the coordinates of all lampposts in Hong Kong are available from the Land Department, were recorded. The ground truth was generated using interpolation between two lampposts with estimated steps from our previous method, which showed an error ratio below 1% [55]. The intervals between two neighboring lampposts varied from 30 to 80 m, and therefore, the accuracy of the ground truth is higher than 1 m. Overall, these experiment sites represent middle- and high-density urban areas with varying road orientations, facilitating an evaluation of the RT-GWSC method's performance under both static and kinematic conditions.

1) Analysis of the RT-GWSC Method: To demonstrate the effectiveness of the proposed method in urban positioning, a detailed analysis of a static experiment was carried out in

Authorized licensed use limited to: Hong Kong Polytechnic University. Downloaded on June 16,2025 at 12:40:55 UTC from IEEE Xplore. Restrictions apply.

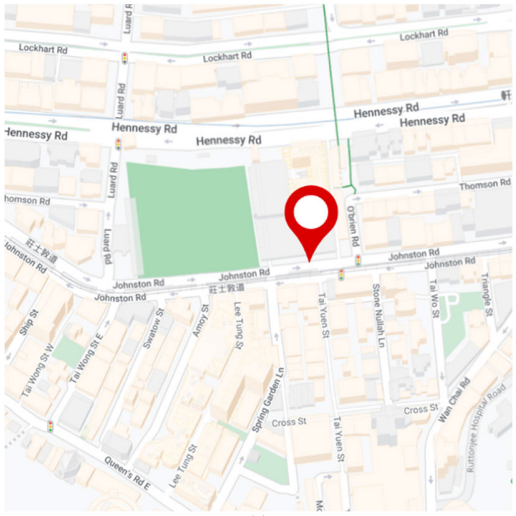

(a)

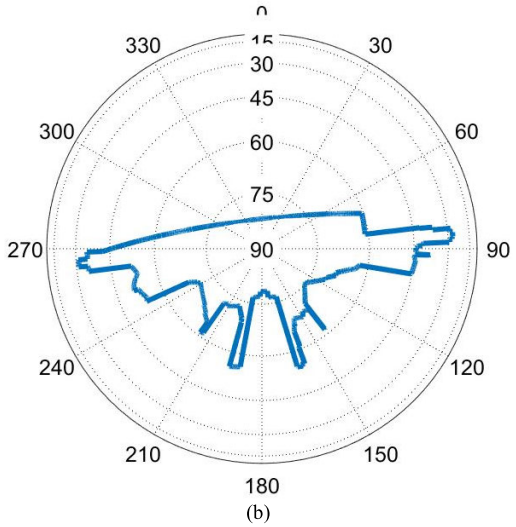

(b)

Fig. 7. Illustration of the visibility boundary at the test point. (a) Location of the receiver. (b) Visibility boundary.

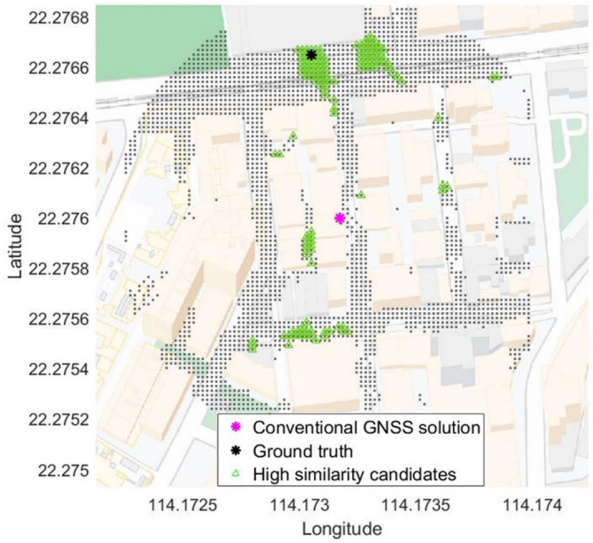

(a)

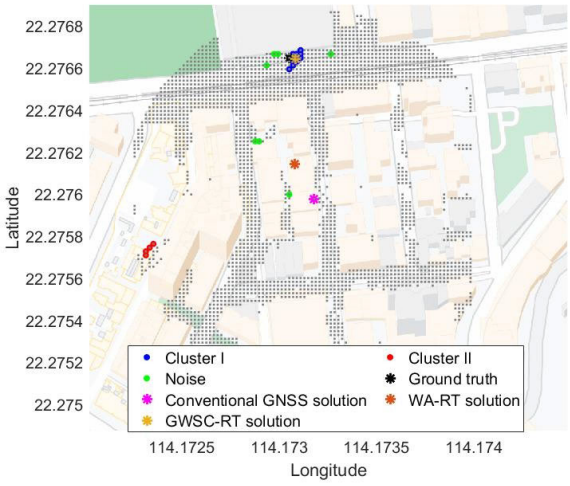

(b)

Fig. 8. Positioning comparison of WA-RT and RT-GWSC methods. (a) Grid weights in one epoch with the selection of high similarity candidates. (b) Positioning solutions of three methods with grid weights after multiepoch grid smoothing and cluster selection after DBSCAN clustering.

the high-urbanized areas. The experiment site is shown in Fig. 7(a), and Fig. 7(b) illustrates the corresponding visibility boundary. The receiver was located near the tall buildings with narrow streets surrounding it, and the receiver is heavily blocked by buildings. The positioning solutions exhibited large errors in the northing direction, varying between 30 and 80 m within 6 min, with an overall horizontal accuracy of 61.5 m.

A single epoch was chosen for a comprehensive analysis. Centered around the results from conventional GNSS, candidates within a specific area could be identified by utilizing the 3-D city database, allowing for the removal of ground points within buildings, as indicated by gray dots in Fig. 8(a), with the black asterisk denoting the true location of receiver and the magenta asterisk representing the original GNSS results. After the calculation of the pseudorange similarities dP_{C_j} on each candidate, candidates displaying high similarity (low differenced residuals) were chosen, as shown with green triangle in Fig. 8(a), revealing that these scattered grids significantly deviated from the ground truth due to the presence of outliers.

In this epoch, the positioning solutions from the conventional GNSS technology contained larger errors in the cross-street direction rather than along-street errors, since the satellites in the cross-street direction are more likely reflected or blocked. By applying the conventional RT technology, the candidates with high weights scattered into several regions due to the remained unmodeled errors in pseudorange DD residuals. The WA-RT technology improves the performance in cross-street direction by removing some southern candidates, but it cannot recognize the optimal regions in one epoch. By accumulating the multiepoch grid weights, invalid candidates were filtered out. Then, by employing the DBSCAN cluster approach, the candidates with high similarities are clustered into three groups, illustrated in Fig. 8(b). It is obvious that the cluster I around the ground truth (black asterisk) is majority; other outliers are filtered out by grid weight smoothing. The results from the proposed approach are depicted as the orange dot, remarkably near to the true location. The traditional WA-RT approach (brown asterisk) slightly enhanced the positioning accuracy of conventional GNSS outputs from 75.5 to 56.2 m, whereas the solution from the GWSC-RT approach achieved the highest accuracy

Authorized licensed use limited to: Hong Kong Polytechnic University. Downloaded on June 16,2025 at 12:40:55 UTC from IEEE Xplore. Restrictions apply.

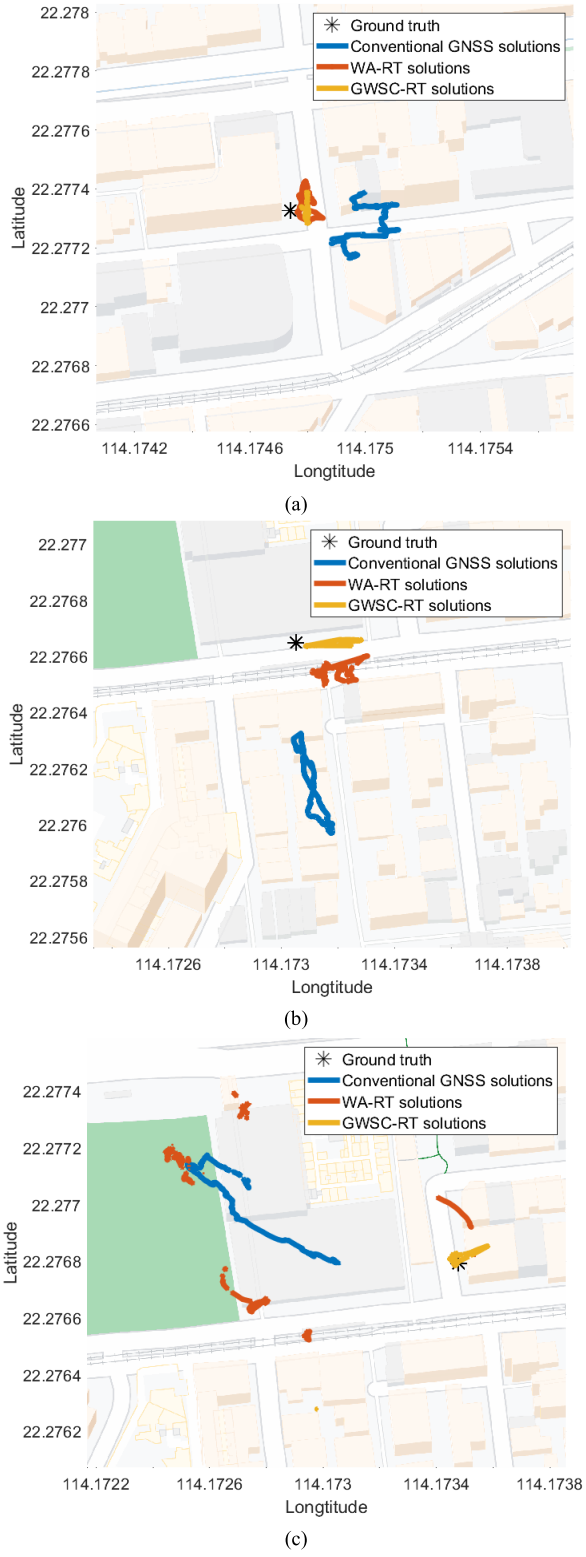

Fig. 9. Comparison of positioning solutions among different methods in three separate urban regions. (a) Static test 1. (b) Static test 2. (c) Static test 3.

of 3.5 m. As a result, the proposed method performs better than WA-RT technology.

2) Evaluation of Positioning Performance: The RT-GWSC approach was then applied to obtain position solutions in three static and one kinematic experiments. First, the comparison of positioning solutions in static tests among conventional GNSS

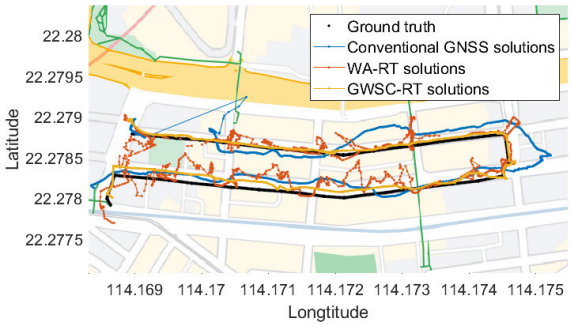

Fig. 10. Comparison of positioning solutions from three approaches under kinematic conditions.

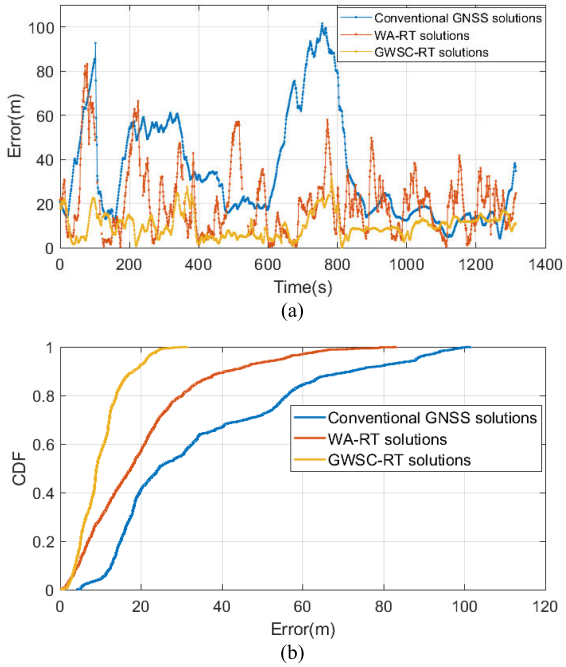

Fig. 11. (a) Comparison of positioning errors from three approaches under kinematic conditions and (b) corresponding cdf of positioning errors.

method, WA-RT method, and RT-GWSC method, is shown in Fig. 9.

The figures illustrate that both RT methods were effective in enhancing the GNSS positioning accuracy under static conditions. Among the outcomes, the proposed RT-GWSC method demonstrated greater robustness in deriving positioning solutions compared to the conventional WA-RT method. Simultaneously, the positioning accuracy from RT-GWSC method presented significant improvement across all three experiments, while the WA-RT approach had a poor performance in the third test.

Subsequently, a kinematic experiment was carried out in densely urbanized regions, where performance of the conventional GNSS degraded with errors up to 100 m, as indicated by the blue line in Figs. 10 and 11(a). The positioning results among the three methods were compared as depicted in Fig. 10, while their positioning errors and their cdf were illustrated in Fig. 11(a) and (b), respectively.

Through the comparison of the positioning results in all static and kinematic tests, the proposed RT-GWSC method notably showed enhancement in the precision in single epoch

Authorized licensed use limited to: Hong Kong Polytechnic University. Downloaded on June 16,2025 at 12:40:55 UTC from IEEE Xplore. Restrictions apply.

TABLE II
POSITIONING ACCURACIES OF THREE METHODS IN ALL EXPERIMENTS

Test type			Static			Kinematic
ID			1	2	3	4
Positioning accuracy (m)	Conventional GNSS method	N	8.4	60.9	29.2	14.7
		E	27.8	8.1	81.3	39.5
		H	29.1	61.5	86.4	42.2
	WA- RT method [38]	N	4.7	12	36.7	14.3
		E	5.6	10.7	86.4	21.0
		H	7.3	16.0	93.9	25.4
	RT GWSC method	N	4.2	0.6	6.3	7.2
		E	6.1	15.0	6.3	8.9
		H	7.4	15.0	8.9	11.4
IR (%)	WA- RT method	H	74.9	74.0	-8.7	39.8
	RT GWSC method	H	74.6	75.6	89.7	73.0

*N, E, H denote the Northing, Easting and Horizontal direction.

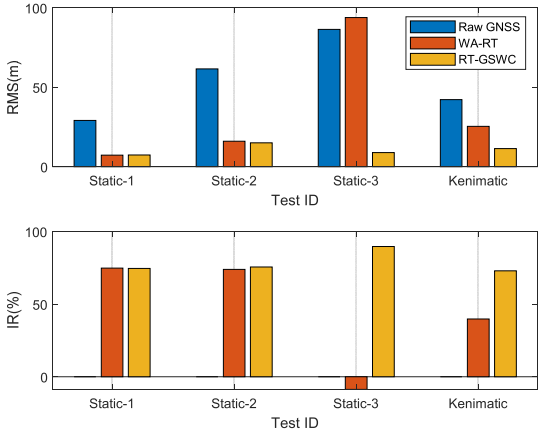

Fig. 12. Comparison of positioning accuracy with IR between three methods (Kalman-based).

positioning, demonstrating greater stability in its positioning solutions. On the other hand, the performance of WA-RT method was inconstant. Although it was effective in some epochs, multiple large errors were exhibited and caused jumps in positioning solutions as observed in Fig. 10. Among the three positioning approaches, the proposed method achieved the highest positioning accuracy with more stable performance. Meanwhile, the improvement rate (IR) was calculated to express the accuracy improvement between conventional GNSS method and the RT-based methods as follows:

$$\mathrm{IR} = \frac{\mathrm{NV} - \mathrm{OV}}{\mathrm{OV}} * 100\% \tag{18}$$

where IR represents improvement rate; NV and OV stand for new and original value from new and original method, respectively.

The positioning accuracy among the three methods and IR of the two RT-based methods are summarized and compared in Table II and Fig. 12.

In static tests, positioning errors of the conventional GNSS method were found between 29.1 and 86.4 m while the WA-RT method showed errors between 7.3 and 93.9 m. In contrast, the proposed method demonstrated a high accuracy with 7.4–15.0 m errors. Moreover, in the kinematic experiment, the positioning accuracy of the conventional GNSS and WA-RT methods was 42.2 and 25.4 m, respectively, whereas it is enhanced to 11.4 m with the proposed method. To sum up, the WA-RT method showed improvement in two of the three statics tests, with IR around 75%. However, its performance degraded in highly dense urban canyons (test 3). Additionally, it provided an IR 36.8% in kinematic test. In contrast, the proposed RT-GWSC method significantly improved the positioning accuracy with IRs ranging from 73% to 89.7% in all four (static and kinematic) experiments. This demonstrates that the proposed method can improve the positioning accuracy and robustness in urban canyons in both static and kinematic setup.

During the static experiments, the WA-RT method demonstrated enhanced positioning accuracy in moderately dense urban areas (static tests 1 and 2), characterized by H/W ratios ranging from 2.1 to 7.5. However, in highly dense urban environments (static test 3) with H/W ratios of 7.9 and 9.8, the WA-RT method exhibited a significant decline in positioning accuracy. Moreover, the WA-RT solutions displayed inconsistencies with several jumps in the positioning results, as depicted in Fig. 9(c). Conversely, the proposed RT-GWSC method showed improvements among all levels of GNSS signal obstruction, particularly in the cross-street directions. In the kinematic test, the WA-RT approach's positioning solutions also exhibited instability with jumps. It presented the improvements in certain cross-street scenarios but performance deteriorated on the third street compared to conventional GNSS solutions. In contrast, the proposed method significantly enhanced positioning performance with consistent accuracy across various urban densities.

To conclude, although the WA-RT method showed the effectiveness in middle dense urban areas, it contained large positioning variation and presented the inconsistency in different level of GNSS signal obstruction. However, the proposed RT-GWSC method showed that the highest positioning accuracy comparing to the conventional GNSS method and WA-RT method reduced the maximum positioning errors and improved positioning robustness. This indicates that the proposed RD model effectively increases the signal simulation rates, inleading to the enhancement in satellites availability, while the proposed positioning scheme improves the robustness of localization.

C. Discussion

The proposed RD model presented a more comprehensive simulation of reflected/diffracted signals, which increases the number of available satellites and further improves the satellite geometry. After the NLOS correction, the unmodeled errors would be remained in pseudorange residuals. The employment of WA method for positioning fails to remove outliers. In contrast, the accumulation of multiepoch weights can augment the weights of the grids around the ground truth since they

Authorized licensed use limited to: Hong Kong Polytechnic University. Downloaded on June 16,2025 at 12:40:55 UTC from IEEE Xplore. Restrictions apply.

are the highest among all epochs, and outliers can be filtered out. With the implementation of DBSCAN clustering method, the optimal cluster was finally determined after removing the noise. On the basis of the RD model and GWSC method, the proposed method is more robust to obtain positioning solutions than WA-RT technology.

IV. Conclusion and Future Work

In this article, the two-stage improvement of RT-based positioning method in dense urban environments has been shown to significantly enhance the accuracy and robustness of GNSS positioning. The first stage, involving a more comprehensive reflection model, improves the success rate of path delay estimation. The second stage addresses unmodeled errors and introduces a novel method, RT-GWSC, aimed at enhancing positioning accuracy. In this stage, after the grid weight calculation with the aid of 3-D model, the PDR technique is integrated with the multiepoch weights from the GNSS-based approach in the grid weighting stage, and DBSCAN clustering analysis is applied to remove outliers, further increasing positioning accuracy and robustness.

Experimental results in various urban setup validate the proposed methods. The enhanced signal simulation method outperforms the traditional method in terms of signal classification, exhibiting greater consistency in reception (NLOS-with-reflection prediction sensitivity from 53.7% to 90.7%, NLOS-without-reflection prediction specificity from 74.4% to 95.7%, and overall prediction accuracy from 86.3% to 96.8%). Furthermore, the estimated delays from the improved estimation method align closely with the received true errors, and the results indicated that the estimation errors for over 95% and 65% of signals were below 15 and 5 m, respectively. A thorough analysis of the proposed GWSC-RT approach was conducted under static and kinematic scenarios within typical dense urbans. In dense urban regions, the positioning accuracies of the raw GNSS outputs deteriorated to tens of meters (ranging from 29.1 to 86.4 m). In contrast, a significant enhancement has been exhibited with current method with accuracy below 15 m, surpassing the performance of the traditional WA-RT positioning solutions. Overall, the experimental results highlight the effectiveness of 3DMA approaches in enhancing positioning performance in multipath scenarios.

However, the efficiency of 3-D model-based approaches is still challenged by high computation load, large storage demands, and dependency on the accuracy and format of 3-D models. Firstly, the inaccurate 3-D model will introduce the wrong reflection prediction. A high-fidelity 3-D model enables better prediction and modeling of multipath effects, but the sophisticated models increase the computational demands. Meanwhile, the pre-generated models are unable to represent the changes of building structures or dynamic interferences, and this limitation can have implications for positioning performance. The proposed method can mitigate these effects by filtering. However, it will still be challenged when the accuracy of 3-D model is too low to simulate the path delays. Secondly, the RT technology demands the high computation loads since it validates the reflection path over each potential reflector. To achieve real-time positioning, enhancement in processing power with system optimization would be needed. Firstly, rather than the use of central processing units (CPUs), the traditional graphics processing unit (GPU) is a powerful engine. With the increase of its processing capabilities, it can be used as a highly parallel programmable processor to accelerate the computing process. Secondly, the path delays for all candidates can be pre-generated and stored in offline stage. As a result, the path delays can be simply extracted from database with the index of selected candidates in the positioning stage. The RT-GWSC method shows the potential to be effectively scaled for larger urban areas with diverse building structures. By utilizing enhanced RD model, this method can accurately simulate signal propagation in complex urban environments, allowing the accommodation of varieties in street widths, building heights, and layouts. Moreover, the optimization of the positioning scheme ensures that the method can maintain high localization accuracy with differing architectural features. The scalability of the RT-GWSC method for larger urban areas relies on the computational efficiency. After the optimization of the data processing, it has the potential to provide real-time positioning solutions in larger and more complicated urban areas, and field tests can be carried out in more diverse scenarios, such as various cities with different building structures and areas with different levels of GNSS signal obstruction. With our previous studies of the integration with inertial sensors, a seamless positioning based on the proposed method will be researched further. Furthermore, considering that 3-D model is not available globally, an efficient approach independent of 3-D models incorporating inertial sensors in low-cost devices could also be investigated to enhance the positioning accuracy in urban canyons in different scenarios.

Fig. 13. Illustration of practical reflection path of satellite ID 22 based on Google Earth.

Appendix

In Fig. 6(a), the predicted delay of satellite ID 22 is inconsistent with the received error, which shows a sudden change. This is caused by the 3-D model error, which is discussed as below.

The current 3-D model contains building surfaces and infrastructures. However, there are many billboards over the road, which are not included in the 3-D model. Fig. 13 shows the actual environments of the target area from Google Earth. Depicted in Fig. 14, the gray planes indicate building surfaces in 3-D city model, green pin is the location of receiver, and

Authorized licensed use limited to: Hong Kong Polytechnic University. Downloaded on June 16,2025 at 12:40:55 UTC from IEEE Xplore. Restrictions apply.

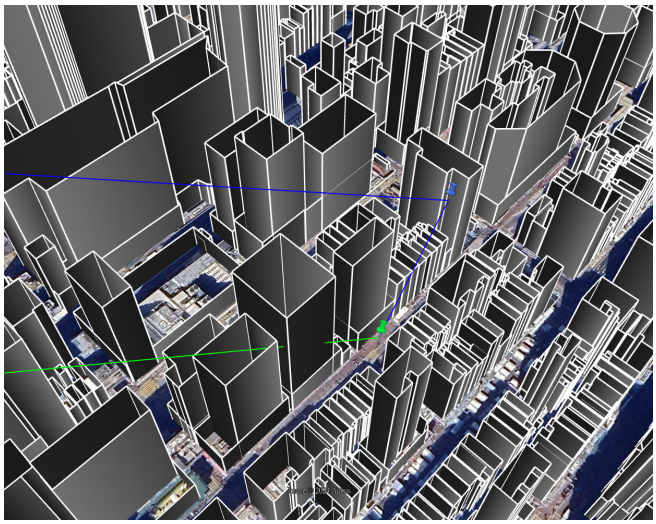

Fig. 14. Illustration of predicted reflection path of satellite ID 22 based on 3-D model.

green line represents the LOS signal of satellite ID 22, which is obviously blocked by the building. Based on the 3-D model, the reflection point is determined, shown as the blue pin. The blue lines are NLOS signal, and the path delays between LOS and predicted NLOS signal is 94.6 m. However, in real-world scenarios, the predicted signal is blocked by the billboard, which is close to the receiver; moreover, the actual reflection point is on the billboard, shown as Fig. 13. In this case, the practical reflection path of satellite 22 is illustrated in Fig. 13, where the red pin is the practical reflection point, and the red line is the reflection path. The corresponding path delay is approximately equal to the received error (14.2 m).

REFERENCES

[1] N. Kubo, K. Kobayashi, L. Hsu, and O. Amai, "Multipath mitigation technique under strong multipath environment using multiple antennas," *J. Aeronaut., Astronaut. Aviation, Ser. A*, vol. 49, no. 1, pp. 75–82, Mar. 2017.

[2] D. H. Won et al., "Selective integration of GNSS, vision sensor, and INS using weighted DOP under GNSS-challenged environments," *IEEE Trans. Instrum. Meas.*, vol. 63, no. 9, pp. 2288–2298, Sep. 2014.

[3] M. Ding, W. Chen, D. Weng, and X. Mi, "Adaptive jamming mitigation in single-antenna receivers with spectral analysis and switchable filtering," *IEEE Trans. Aerosp. Electron. Syst.*, vol. 60, no. 5, pp. 5891–5905, Oct. 2024, doi: 10.1109/TAES.2024.3397290.

[4] C. Jiang et al., "Smartphone PDR/GNSS integration via factor graph optimization for pedestrian navigation," *IEEE Trans. Instrum. Meas.*, vol. 71, pp. 1–12, 2022, doi: 10.1109/TIM.2022.3186082.

[5] J. Wang, D. Weng, X. Qu, W. Ding, and W. Chen, "A novel deep odometry network for vehicle positioning based on smartphone," *IEEE Trans. Instrum. Meas.*, vol. 72, pp. 1–12, 2023, doi: 10.1109/TIM.2023.3240227.

[6] C. Boucher and J.-C. Noyer, "A hybrid particle approach for GNSS applications with partial GPS outages," *IEEE Trans. Instrum. Meas.*, vol. 59, no. 3, pp. 498–505, Mar. 2010.

[7] M. Petovello and P. Groves, "Multipath vs. NLOS signals," *Inside GNSS*, vol. 8, no. 6, pp. 40–42, 2013.

[8] S. Schön et al., "Towards integrity for GNSS-based urban navigation—Challenges and lessons learned," in *Proc. IEEE Intell. Vehicles Symp. (IV)*, Aachen, Germany, Jun. 2022, pp. 1774–1781, doi: 10.1109/IV51971.2022.9827402.

[9] L.-T. Hsu, "Analysis and modeling GPS NLOS effect in highly urbanized area," *GPS Solutions*, vol. 22, no. 1, pp. 7–18, Jan. 2018.

[10] L. Garin and J.-M. Rousseau, "Enhanced strobe correlator multipath rejection for code & carrier," in *Proc. 10th Int. Tech. Meeting Satell. Division Inst. Navig.*, Kansas City, MO, USA, Sep. 1997, pp. 559–568.

[11] M. G. Amin and W. Sun, "A novel interference suppression scheme for global navigation satellite systems using antenna array," *IEEE J. Sel. Areas Commun.*, vol. 23, no. 5, pp. 999–1012, May 2005.

[12] G. A. McGraw, R. S. Y. Young, K. Reichenauer, J. Stevens, and F. Ventrone, "GPS multipath mitigation assessment of digital beam forming antenna technology in a JPALS dual frequency smoothing architecture," in *Proc. Nat. Tech. Meeting Inst. Navig.*, San Diego, CA, USA, Jan. 2004, pp. 561–572.

[13] Z. Jiang and P. D. Groves, "NLOS GPS signal detection using a dual-polarisation antenna," *GPS Solutions*, vol. 18, no. 1, pp. 15–26, Jan. 2014.

[14] P. Xie and M. G. Petovello, "Improving high sensitivity receiver performance in multipath environment for vehicular applications," in *Proc. 25th Int. Tech. Meeting Satell. Division Inst. Navig.*, Nashville, TN, USA, Sep. 2012, pp. 448–458.

[15] A. Kumar and A. K. Singh, "A novel multipath mitigation technique for GNSS signals in urban scenarios," *IEEE Trans. Veh. Technol.*, vol. 69, no. 3, pp. 2649–2658, Mar. 2020, doi: 10.1109/TVT.2019.2962919.

[16] Z. Yan, X. Chen, X. Tang, and X. Zhu, "Design and performance evaluation of the improved INS-assisted vector tracking for the multipath in urban canyons," *IEEE Trans. Instrum. Meas.*, vol. 71, pp. 1–16, 2022.

[17] M. Ding, X. Mi, W. Chen, D. Weng, and W. Ding, "Equalization of frequency domain adaptive filter (FDAF) using signal prediction aided reference spectrum model (SPRSM)," *IEEE Trans. Instrum. Meas.*, vol. 73, pp. 1–16, 2024, doi: 10.1109/TIM.2024.3366269.

[18] T. Iwase, N. Suzuki, and Y. Watanabe, "Estimation and exclusion of multipath range error for robust positioning," *GPS Solut.*, vol. 17, pp. 53–62, Jan. 2013.

[19] Z. Jiang, P. D. Groves, W. Y. Ochieng, S. Feng, C. Milner, and P. G. Mattos, "Multi-constellation GNSS multipath mitigation using consistency checking," in *Proc. 24th Int. Tech. Meeting Satell. Division Inst. Navig.*, Portland, OR, USA, Sep. 2011, pp. 3889–3902.

[20] Z. Jiang and P. D. Groves, "GNSS NLOS and multipath error mitigation using advanced multi-constellation consistency checking with height aiding," in *Proc. 25th Int. Tech. Meeting Satell. Division Inst. Navig.*, Nashville, TN, USA, Sep. 2012, pp. 79–88.

[21] L.-T. Hsu, H. Tokura, N. Kubo, Y. Gu, and S. Kamijo, "Multiple faulty GNSS measurement exclusion based on consistency check in urban canyons," *IEEE Sensors J.*, vol. 17, no. 6, pp. 1909–1917, Mar. 2017.

[22] Y. Wen, W. Dai, W. Yu, and L. Pan, "Mitigation of multiple outliers using consistency checking for GNSS standard point positioning in urban areas," *Adv. Space Res.*, vol. 73, no. 3, pp. 1721–1733, Feb. 2024.

[23] P. D. Groves and Z. Jiang, "Height aiding, C/N0 weighting and consistency checking for GNSS NLOS and multipath mitigation in urban areas," *J. Navigat.*, vol. 66, no. 5, pp. 653–669, Sep. 2013.

[24] D. Weng, M. Cai, W. Chen, J. Wang, and S. Ji, "GNSS fault detection and exclusion (FDE) under sidewalk constraints for pedestrian localization in urban canyons," *IEEE Trans. Intell. Transp. Syst.*, vol. 25, no. 9, pp. 11168–11179, Sep. 2024.

[25] R. Sun, X. Huang, Q. Cheng, and W. Yotto Ochieng, "A novel GNSS quality control method with satellite geometric network for dynamic urban positioning," *IEEE Trans. Instrum. Meas.*, vol. 73, pp. 1–13, 2024.

[26] P. D. Groves, "Shadow matching: A new GNSS positioning technique for urban canyons," *J. Navig.*, vol. 64, no. 3, pp. 417–430, Jun. 2011.

[27] L. Wang, P. D. Groves, and M. K. Ziebart, "GNSS shadow matching: Improving urban positioning accuracy using a 3D city model with optimized visibility scoring scheme," *Navigation*, vol. 60, no. 3, pp. 195–207, Sep. 2013.

[28] L. Wang, P. D. Groves, and M. K. Ziebart, "Smartphone shadow matching for better cross-street GNSS positioning in urban environments," *J. Navigat.*, vol. 68, no. 3, pp. 411–433, 2015.

[29] M. Adjrad and P. D. Groves, "Intelligent urban positioning: Integration of shadow matching with 3D-mapping-aided GNSS ranging," *J. Navigat.*, vol. 71, no. 1, pp. 1–20, Jan. 2018.

[30] H. Luo, D. Weng, and W. Chen, "An improved shadow matching method for smartphone positioning," *Geomatics Inf. Sci. Wuhan Univ.*, vol. 46, no. 12, pp. 1907–1915, Dec. 2021.

[31] S. Bhamidipati, S. Kousik, and G. Gao, "Set-valued shadow matching using zonotopes for 3D-map-aided GNSS localization," *Navig., J. Inst. Navigat.*, vol. 69, no. 4, p. 547, Dec. 2022.

[32] H.-F. Ng, G. Zhang, and L.-T. Hsu, "Robust GNSS shadow matching for smartphones in urban canyons," *IEEE Sensors J.*, vol. 21, no. 16, pp. 18307–18317, Aug. 2021.

[33] A. Bourdeau, M. Sahmoudi, and J.-Y. Tourneret, "Constructive use of GNSS NLOS-multipath: Augmenting the navigation Kalman filter with a 3D model of the environment," in *Proc. 15th Int. Conf. Inf. Fusion*, Jul. 2012, pp. 2271–2276.

Authorized licensed use limited to: Hong Kong Polytechnic University. Downloaded on June 16,2025 at 12:40:55 UTC from IEEE Xplore. Restrictions apply.

[34] L.-T. Hsu, Y. Gu, and S. Kamijo, "NLOS correction/exclusion for GNSS measurement using RAIM and city building models," *Sensors*, vol. 15, no. 7, pp. 17329–17349, Jul. 2015.
[35] P. D. Groves and M. Adjrad, "Performance assessment of 3D-mapping–aided GNSS Part 1: Algorithms, user equipment, and review," *Navigation*, vol. 66, no. 2, pp. 341–362, Mar. 2019.
[36] T. Suzuki and N. Kubo, "Correcting GNSS multipath errors using a 3D surface model and particle filter," in *Proc. 26th Int. Tech. Meeting Satell. Division Inst. Navig.*, Nashville, TN, USA, Sep. 2013, pp. 1583–1595.
[37] R. Kumar and M. G. Petovello, "A novel GNSS positioning technique fors improved accuracy in urban canyon scenarios using 3D city model," in *Proc. 27th Int. Tech. Meeting Satell. Division Inst. Navig.*, Tampa, FL, USA, Sep. 2014, pp. 2139–2148.
[38] L.-T. Hsu, Y. Gu, and S. Kamijo, "3D building model-based pedestrian positioning method using GPS/GLONASS/QZSS and its reliability calculation," *GPS Solutions*, vol. 20, no. 3, pp. 413–428, Jul. 2016.
[39] H.-F. Ng, G. Zhang, and L.-T. Hsu, "A computation effective range-based 3D mapping aided GNSS with NLOS correction method," *J. Navigat.*, vol. 73, no. 6, pp. 1202–1222, Nov. 2020.
[40] H.-F. Ng, G. Zhang, Y. Luo, and L.-T. Hsu, "Urban positioning: 3D mapping-aided GNSS using dual-frequency pseudorange measurements from smartphones," *Navigation*, vol. 68, no. 4, pp. 727–749, Dec. 2021.
[41] Q. Zhong and P. D. Groves, "Multi-epoch 3D-mapping-aided positioning using Bayesian filtering techniques," *Navig., J. Inst. Navigat.*, vol. 69, no. 2, p. 515, Jun. 2022.
[42] L. Zhang, H.-F. Ng, G. Zhang, and L.-T. Hsu, "Ray-tracing correction for GNSS velocity estimation using Doppler frequency: A feasibility analysis," *IEEE Trans. Instrum. Meas.*, vol. 73, pp. 1–10, 2024.
[43] Z. Lyu and Y. Gao, "An efficient pixel shader-based ray-tracing method for correcting GNSS non-line-of-sight error with large-scale surfaces," *GPS Solutions*, vol. 27, no. 4, p. 159, Jul. 2023.
[44] R. Pugliese, D. Hai, and D. Abel, "Non-line-of-sight GNSS ray tracing and rectification in urban canyons by LiDAR-based surface reconstruction," in *Proc. Int. Tech. Meeting Inst. Navigat.*, Long Beach, CA, USA, Feb. 2023, pp. 124–137.
[45] R. Hu, W. Wen, and L.-T. Hsu, "Fisheye camera aided GNSS NLOS detection and learning-based pseudorange bias correction for intelligent vehicles in urban canyons," in *Proc. IEEE 26th Int. Conf. Intell. Transp. Syst. (ITSC)*, Bilbao, Spain, Sep. 2023, pp. 6088–6095.
[46] H.-Y. Ho, H.-F. Ng, Y.-T. Leung, W. Wen, L.-T. Hsu, and Y. Luo, "Smartphone level indoor/outdoor ubiquitous pedestrian positioning 3DMA GNSS/VINS integration using FGO," *Int. Arch. Photogramm., Remote Sens. Spatial Inf. Sci.*, vol. 1, pp. 175–182, May 2023.
[47] G. Zhang and L. Hsu, "Performance assessment of GNSS diffraction models in urban areas," *Navigation*, vol. 68, no. 2, pp. 369–389, Jun. 2021.
[48] S. Miura, S. Hisaka, and S. Kamijo, "GPS multipath detection and rectification using 3D maps," in *Proc. 16th Int. IEEE Conf. Intell. Transp. Syst. (ITSC)*, Oct. 2013, pp. 1528–1534, doi: 10.1109/ITSC.2013.6728447.
[49] K. M. Larson, J. J. Braun, E. E. Small, V. U. Zavorotny, E. D. Gutmann, and A. L. Bilich, "GPS multipath and its relation to near-surface soil moisture content," *IEEE J. Sel. Topics Appl. Earth Observ. Remote Sens.*, vol. 3, no. 1, pp. 91–99, Mar. 2010, doi: 10.1109/JSTARS.2009.2033612.
[50] H. Luo, "High precision positioning for pedestrian navigation in dense urban environments," Ph.D. dissertation, Dept. LSGI, Hong Kong Polytech. Univ., Hong Kong, 2022.
[51] H. S. Hopfield, "Tropospheric range error parameters: Further studies," Dept. Appl. Phys. Lab., Johns Hopkins Univ., Baltimore, MD, USA, Tech. Rep. APL/JHU CP 015, 1972.
[52] J. A. Klobuchar, "Ionospheric time-delay algorithm for single-frequency GPS users," *IEEE Trans. Aerosp. Electron. Syst.*, vol. AES-23, no. 3, pp. 325–331, May 1987.
[53] U. Robustelli, M. Cutugno, J. Paziewski, and G. Pugliano, "GNSS-SDR pseudorange quality and single point positioning performance assessment," *Appl. Geomatics*, vol. 15, no. 3, pp. 583–594, Sep. 2023.
[54] L.-T. Hsu, "GNSS multipath detection using a machine learning approach," in *Proc. IEEE 20th Int. Conf. Intell. Transp. Syst. (ITSC)*, Oct. 2017, pp. 1–6.
[55] H. Luo et al., "Integration of GNSS and BLE technology with inertial sensors for real-time positioning in urban environments," *IEEE Access*, vol. 9, pp. 15744–15763, 2021, doi: 10.1109/ACCESS.2021.3052733.
[56] M. Ester, H. Kriegel, J. Sander, and X. Xu, "A density-based algorithm for discovering clusters in large spatial databases with noise," in *Proc. KDD*, Munich, Germany, Jan. 1996, pp. 226–231.

Huan Luo received the B.Sc. and M.Sc. degrees in geomatics engineering from Northeastern University, Shenyang, China, in 2013 and 2015, respectively, and the Ph.D. degree from The Hong Kong Polytechnic University, Hong Kong, in 2022.

She is currently a Post-Doctoral Fellow with the Department of Land Surveying and Geo-Informatics, The Hong Kong Polytechnic University. Her research interests include global navigation satellite system (GNSS) positioning in challenging environments, multipath mitigation, and multisensor integration for pedestrian localization.

Xiaolong Mi received the dual Ph.D. degree from the University of Chinese Academy of Sciences, Beijing, China, in 2022, and Curtin University, Bentley, WA, Australia, in 2023.

He is currently a Research Assistant Professor at the Department of Land Surveying and Geo-Informatics, The Hong Kong Polytechnic University, Hong Kong. His research interests include global navigation satellite system (GNSS) and low Earth orbit (LEO) technologies for positioning, navigation, and timing (PNT) along with the application of artificial intelligence (AI) in the Earth and space sciences.

Yang Yang is currently a Research Assistant Professor at The Hong Kong Polytechnic University, Hong Kong. He has been actively working on global navigation satellite system (GNSS)-related research for over ten years. His research mainly focuses on GNSS reflectometry for remote sensing, GNSS passive radar, GNSS synthetic aperture radar, GNSS software-defined-radio receiver, signal of opportunities, and GNSS multipath analysis.

Wu Chen received the Ph.D. degree from Newcastle University, Newcastle upon Tyne, U.K., in 1992.

He is currently a Chair Professor of satellite navigation with the Department of Land Surveying and Geo-Informatics, The Hong Kong Polytechnic University, Hong Kong. He has been actively working on global navigation satellite system (GNSS)-related research for more than 30 years. His main research interests include GNSS positioning quality evaluation, system integrity, various GNSS applications, seamless positioning, and simultaneous localization and mapping (SLAM).

Duojie Weng received the B.S. and M.S. degrees in electrical engineering from Hohai University, Nanjing, China, in 2007 and 2010, respectively, and the Ph.D. degree from The Hong Kong Polytechnic University, Hong Kong, in 2016.

He is currently an Assistant Professor with Shenzhen University, Shenzhen, China. His research interests include urban positioning, integrity monitoring of global navigation satellite system (GNSS), kinematic GPS, and sensor integration for various navigation systems.

Authorized licensed use limited to: Hong Kong Polytechnic University. Downloaded on June 16,2025 at 12:40:55 UTC from IEEE Xplore. Restrictions apply.